Nanoscale

Accepted Manuscript

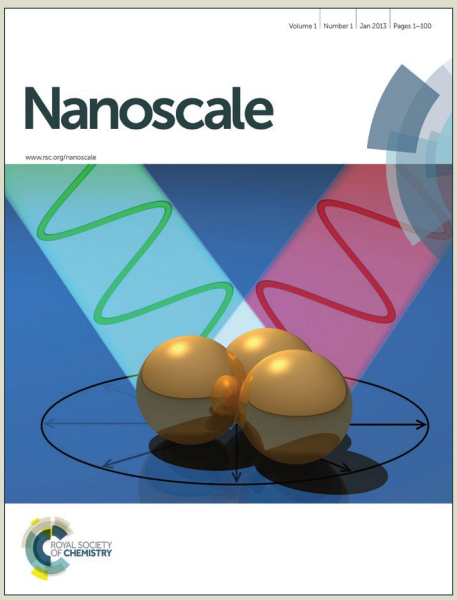

ROYAL SOCIETY OF CHEMISTRY

www.rsc.org/nanoscale

Recent advances in alternative counter electrode materials for Co-mediated dye-sensitized solar cells

Sining Yun*[a], Yanfang Liu[a], Taihong Zhang[a], and Shahzada Ahmad[b]

[a] Functional Materials Laboratory (FML), School of Materials & Mineral Resources, Xi'an University of Architecture and Technology, Xi'an, Shaanxi, 710055, China

E-mail: alexsyun1974@aliyun.com; yunsining@xauat.edu.cn

[b] Abengoa Research, C/ Energía Solar n° 1, Campus Palmas Altas-41014, Sevilla, Spain.

Abstract: Recently, considerable attention has been paid to dye-sensitized solar cells (DSSCs) which are based on Co^{2+}/Co^{3+} redox shuttles, because of their unparalleled merits including higher redox potential, the reduced corrosiveness towards metallic conductors, low costs and high power conversion efficiencies (PCE) (13%). The counter electrode (CE) is an essential component in DSSCs, and plays a crucial role in catalyzing Co^{3+} ion reduction in Co-based DSSCs. In this mini-review, we review recent developments in CE materials for Co-mediated DSSCs including: noble metal platinum (Pt), carbon materials, transition metal compounds (TMCs), polymers, and their corresponding hybrids, highlighting important contributions worldwide that promise low-cost, efficient, and robust Co-mediated DSSC systems. Additionally, the crucial challenges associated with employing these low-cost CE catalysts for Co-based redox couples in DSSCs are stressed.

Keywords: Co^{2+}/Co^{3+} redox shuttles, counter electrode, dye-sensitized solar cells, energy conversion.

1. Introduction

Solar energy, as a clean and renewable energy source, has unparalleled advantages over other energy production methods. In 1991, Grätzel et al developed a new photochemical solar cell using dye-sensitization on TiO_2 mesostructured layers, resulting in the development of dye-sensitized solar cells (DSSCs).[1] Due to their advantages including low cost, choice of color, light weight, packaging technology, environmentally friendly materials, and acceptable photoelectric conversion efficiency, DSSCs are considered to be a promising photovoltaic technology.

Early DSSCs consisted of a TiO_2 photoanode, a CE and an electrolyte solution containing iodide/triiodine (I^-/I_3^-) redox shuttle. It is well known that the photovoltaic parameters of DSSCs, such as open-circuit voltage (V_{oc}), short-circuit current density (J_{sc}) and power conversion efficiency (PCE), are closely related to the electrolyte solution.[2] An impressive PCE of 11% has been achieved by the use of the I^-/I_3^- redox shuttle in DSSCs.[3] However, the I^-/I_3^- electrolyte solution suffers from several problems, for instance, a significant loss in J_{sc} and V_{oc}, the corrosion of Pt CEs and absorption of visible light.[4-7] Meanwhile, the oxidation potential based on the I^-/I_3^- redox shuttle ($E_0(I^-/I_3^-)$) was assumed to be 0.35 V vs standard hydrogen electrode (SHE) and the dye oxidation potential was mostly 1.0 V vs SHE. The relatively negative redox potential based on the I^-/I_3^- redox shuttle limited the V_{oc} and the PCE of the device.[8]

To overcome these issues, Co^{2+}/Co^{3+}, $SeCN^-/(SeCN)$, $SCN^-/(SCN)_2$, Br^-/Br_3^-, and disulfide/thiolate have been investigated as alternative redox shuttles for DSSCs.[9-16] Among them, the Co^{2+}/Co^{3+} redox shuttles have attracted the most attention due to its

unparalleled merits including higher redox potential, and the reduced corrosiveness towards metallic conductors. In addition, when employing Co^{2+}/Co^{3+} redox shuttles in the wavelength range of 440 nm-620 nm, the photon-to-current conversion efficiency (IPCE) values similar to those of the I^-/I_3^- redox system are achieved, and DSSCs assembled with the cyclopentadithiophene-bridged donor-acceptor dye (Y123) with Co^{2+}/Co^{3+} redox shuttles has an enhanced photocurrent response in the 390 nm-480 nm range due to the lower molar absorption coefficients of Co^{2+}/Co^{3+} in the blue spectral region, as seen in **Fig. 1**(**a**). These resulted higher V_{oc} value and an increase in overall PCE (**Fig. 1**(**b**)). Particularly, at lower light intensities, the higher PCE values were measured based on the Co^{2+}/Co^{3+} redox shuttles.[9-10, 17-19] The devices fabricated using an organic dye (SM315) in conjunction with a tris(2,2'-bipyridine) Co^{2+}/Co^{3+} redox shuttles, produced a remarkable PCE of 13.0%, which remains as the benchmark PCE value for liquid electrolyte solution DSSCs.[20] However, some issues still limit the efficiency of Co-mediated DSSCs. The larger size of the Co^{2+}/Co^{3+} redox shuttles, for instance, results in the lower ion mobility and thus limit mass transport. In addition, the inefficient charge transfer of the Co^{2+}/Co^{3+} redox shuttles at the CE also limits the PCE.[21-22]

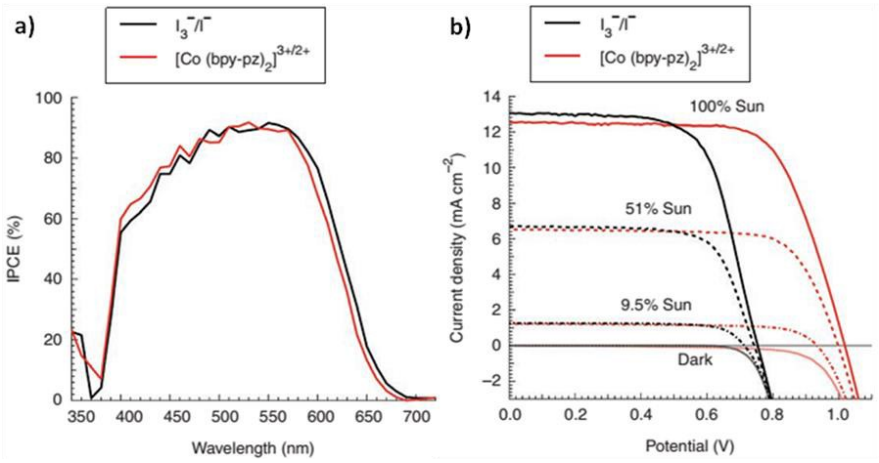

Fig. 1. a) The IPCE spectra for Co^{2+}/Co^{3+} (red lines) and I^-/I_3^- (black lines) redox systems b) Photocurrent density-voltage (*J-V*) curves for the Co^{2+}/Co^{3+} (red lines) and I^-/I_3^- (black lines) DSSCs. Reprinted with permission from ref.[23] Copyright 2012, Nature.

The CE has played a crucial role in the work process of DSSC technologies. The function of the CE is to collect electrons from the external circuit and to reduce the Co^{3+} ion in the electrolyte solution. In the DSSC system, the CE materials should possess high catalytic activity and electrical conductivity. Carbon materials, transition metal compounds (TMCs), conductive polymers, and hybrids have been tested as alternatives to the Pt CE in I-mediated DSSCs.[2, 15, 24-27] However, in-depth analysis and a fundamental understanding of the underlying principles of CE design and operation for Co-mediated DSSCs is lacking in the previous review, which limits the systematic implementation of optimized parameters. Moreover, the rapid increase of research in this area has resulted in an abundance of literature; the implications of these recent developments need to be communicated to the wider scientific community to stimulate further progress. A full understanding of the operational principles in a CE of Co-mediated DSSCs is very important for designing new CEs with improved catalytic activity and stability. In this mini-review, we discuss various

kinds of CEs for the Co-mediated DSSC system, including Pt, carbon materials, TMCs, conductive polymers and hybrids. The advantages and disadvantages of the alternative Pt catalyst are highlighted. Furthermore, the challenges of the high-performance and low-cost Pt-free CEs in Co-mediated DSSCs are also discussed.

2. Working principle of Counter Electrode

2.1. Co-mediators with various ligands

Compared with conventional the I^-/I_3^- redox shuttle, the Co^{2+}/Co^{3+} redox shuttles can be molecularly designed with various ligands such as bipyridine-, terpyridine- and phenanthroline.[10, 28] The structures of the various alternate Co^{2+}/Co^{3+} redox shuttles used in DSSCs are shown in **Fig. 2**.[29] By changing the ligands, the electrochemical and physical properties of the Co^{2+}/Co^{3+} redox shuttles can be easily tuned. The introduction of electron-withdrawing groups on the ligands can increase the redox potential of the Co^{2+}/Co^{3+} redox shuttles, thereby increasing V_{oc} and PCE. Additionally, the large volume of the Co^{2+}/Co^{3+} redox shuttles allow for many catalytically active positions on the non-Pt catalyst surface to be provided, which improves catalytic activity.[12] However, the large volume of the Co^{2+}/Co^{3+} redox shuttles lead to difficulties in diffusion of ions.

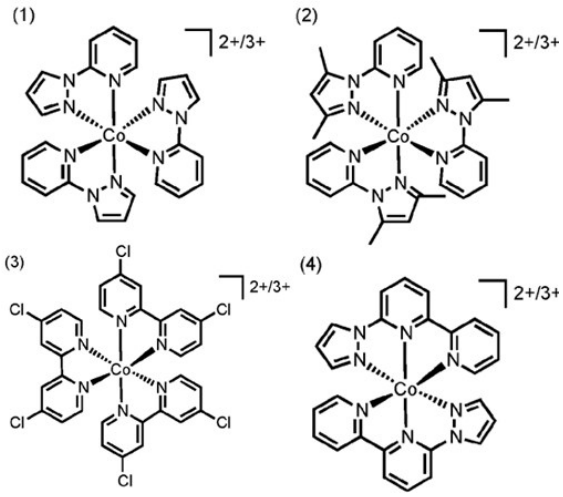

Fig. 2. Structures of the Co-mediated shuttles (1) $[Co(py\text{-}pz)_3](PF_6)_2/[Co(py\text{-}pz)_3](PF_6)_3$; (2) $[Co(py\text{-}pzMe_2)_3](PF_6)_2/[Co(py\text{-}pzMe_2)_3](PF_6)_3$; (3) $[Co(Cl_2bpy)_3](PF_6)_2/[Co(Cl_2bpy)_3](PF_6)_3$; (4) $[Co(bpy\text{-}pz)_2](PF_6)_2/[Co(bpy\text{-}pz)_2](PF_6)_3$, $[Co(bpy\text{-}pz)_2](B(CN)_4)_2/[Co(bpy\text{-}pz)_2](B(CN)_4)_3$, $[Co(bpy\text{-}pz)_2](TFSI)_2/[Co(bpy\text{-}pz)_2](TFSI)_3$. Reprinted with permission from ref.[29] Copyright 2012, Royal Society of Chemistry

2.2 Operational principle of Co-based DSSCs

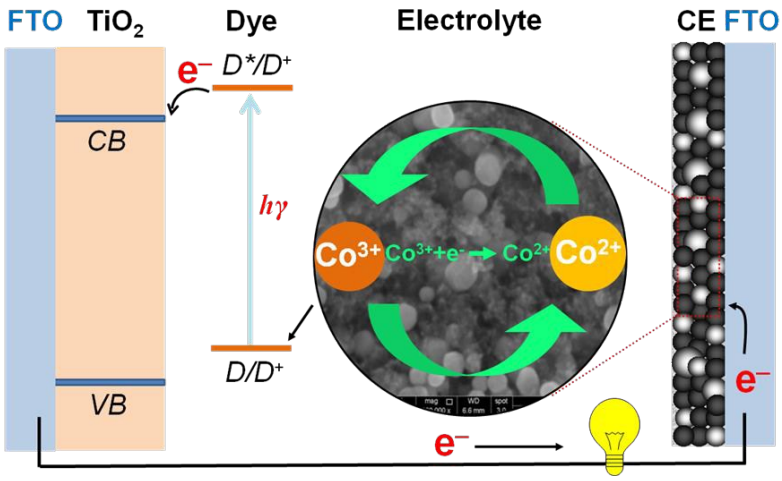

Fig. 3. Schematic drawing of DSSCs based on Co-mediated system

A schematic drawing of a DSSC based on Co-mediated system is shown in **Fig. 3**. The electrolyte solution in a DSSC system contains Co^{2+}/Co^{3+} redox shuttles dissolved in an organic solvent. First, Co^{3+} ion is absorbed on the surface of the CE (Eqn. 1). Under illumination, the dye experiences an electronic excitation from highest occupied molecular orbital (HOMO) to the lowest unoccupied molecular orbital (LUMO) and a sensitizer molecule is excited.[25] Meanwhile, a photoelectron

will be released and injected into the conduction band of the semiconductor, leaving the dye in an oxidized state. Second, the electrons flow from the photoanode to the external load and are then collected at the CE surface. The electrolyte solution is responsible for the regeneration of the oxidized dye by Co^{3+} reduction. The oxidized dye is restored to its original state by electron transfer from the electrolyte solution. The charge transfer reaction was catalyzed by the CE materials. In addition, the electrolyte solution acts as an electron donor. During the process of a regenerative cycle in the DSSC system, the Co^{3+} reduction to Co^{2+} takes place on the surface of the CE, which is significant for the PCE of DSSCs (Eqn. 2)[28]. Finally, the Co^{2+} molecule diffuses from the CE to the electrolyte solution (Eqn. 3).

$$Co^{3+} + CE \rightarrow Co^{3+}(CE) \quad (1)$$

$$Co^{3+}(CE) + e^{-} \rightarrow Co^{2+}(CE) \quad (2)$$

$$Co^{2+}(CE) \rightarrow Co^{2+} \quad (3)$$

The CE strongly influences the fill factor (*FF)* and subsequently the PCE of the devices. The CE must be catalytically active for the reaction and to reduce the overpotential, which drives the reaction at a certain current density.[30] For this purpose, the CE should have low resistance and a high electrocatalytic activity so that the electrode reaction will maintain a low over voltage and energy loss in the DSSCs.[31] Moreover, CEs with a higher specific surface area not only provide more catalytic sites for Co^{3+} reduction, but are also favorable for the regeneration of the sensitizer. The CE should be selected and designed to maximize these synergistic effects in the DSSCs.

3. Counter electrodes (CEs) of Co-mediated DSSCs

3.1 Pt CE

To date, Pt has been recognized as a preferred CE material in I-mediated DSSCs. Pt nanoparticles have several superior properties, such as high surface area, high transmittance, low charge transfer resistance (R_{ct}), and high electrical conductivity. The high surface area of the Pt nanoparticles provides for a large number of active sites available for the redox shuttle, which increases the current density.[25, 32-33]

During the past several decades, many researches have focused on platinized electrodes in conjunction with Co^{2+}/Co^{3+} redox shuttles in DSSCs. The platinized electrode in Co-mediated DSSCs employing a Y123 sensitizer had better performance, as seen in **Fig. 4**(**a**), and the values of V_{oc}, J_{sc}, *FF* and PCE were 901 mV, 15.2 mA cm^{-2}, 0.66, and 9.0%, respectively.[34-35] Meanwhile, an efficient DSSC based on $Co(bpy)_3]^{2+/3+}$, $[Co(dmb)_3]^{2+/3+}$ and $[Co(dtb)_3]^{2+/3+}$ redox shuttle was reported.[19] **Figure 4**(**b**) shows the IPCE for DSSCs sensitized with a syngerstic D-π-A organic sensitizer (D35). In the 360nm-460 nm spectral range, the IPCE for the Co^{2+}/Co^{3+} redox shuttles was higher than that for the I^-/I_3^- redox shuttle. In the case where the DSSC is illuminated from the CE side, instead of working electrode, the effect is even more distinct. Among the different redox shuttles employed, the $[Co(bpy)_3]^{2+/3+}$ in combination with D35 dye gave the highest efficiency of 6.7%, as seen in **Fig. 4**(**c**). The redox potential of the $[Co(bpy)_3]^{2+/3+}$ (0.56 V vs SHE) was higher than that of I^-/I_3^- redox shuttle, which drived the recombination between electrons in the conduction band of the TiO_2 and Co^{2+}/Co^{3+} redox shuttles in the electrolyte solution.

However, fast recombination appeared to be limited when used in combination with D35. Due to a decreased amount of adsorbed Li cations at the TiO_2 surface led to a negative shift of in conduction band, the high V_{oc} based on the two redox shuttles were achieved. For the $[Co(bpy)_3]^{2+/3+}$ redox shuttle, the insulating effect of the alkoxyl groups and the more positive potential of the Co-based redox shuttles led to remarkably higher V_{oc} (0.88 V). Additionally, the use of a one-electron Co^{2+}/Co^{3+} redox shuttles with a more positive redox potential than the I^-/I_3^- redox shuttle was found to achieve higher dark current densities.

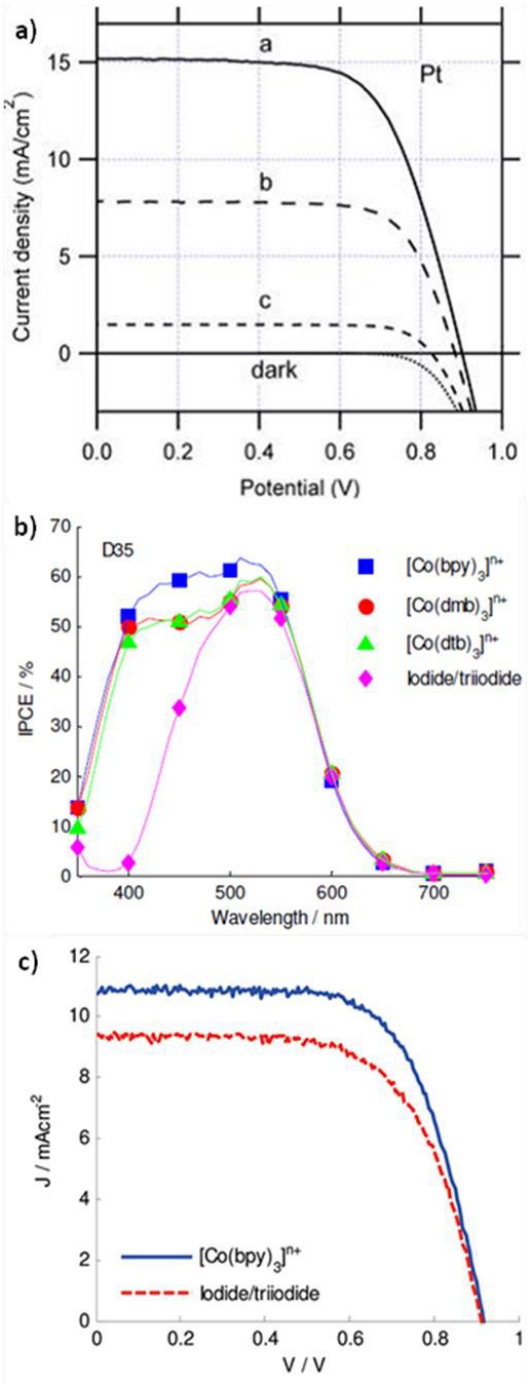

Fig. 4. a) *J-V* characteristics of Pt CE with Y-123 sensitized TiO_2 photoanode in acetonitrile solution of $Co(bpy)_3^{3+/2+}$. Reprinted with permission from ref.[34] Copyright 2012, American Chemical Society. b) Comparison of the IPCE based on different electrolyte solution for DSSCs sensitized with D35. Reprinted with permission from ref.[19] Copyright 2010, American Chemical Society. c) *J-V* characteristics of D35-sensitized solar cells for I- and Co-based redox shuttles under 1000 Wm^{-2} AM1.5G. Reprinted with permission from ref.[19] Copyright 2010, American Chemical Society.

In 2011, using an zinc porphyrin dye (YD2-o-C8), which has excellent

light-harvesting properties, as a sensitizer, M. Grätzel et al. compared the tris(2,2'-bipyridine) Co^{2+}/Co^{3+} redox shuttles with the I^-/I_3^- redox shuttle. The PCE values based on the Co^{2+}/Co^{3+} redox shuttles increased from 7.6% to 11.9%. Further, when using YD2-o-C8 and Y123 in Co^{2+}/Co^{3+} redox shuttles, V_{oc}, J_{sc}, *FF*, and PCE were found to achieve notable values of 935 mV, 17.66 mA cm^{-2}, 0.74, and 12.3%, respectively.[36] These remarkable results indicated that the co-sensitizer had well-aligned energy levels with the Co^{2+}/Co^{3+} redox shuttles. The lower rate of electron recapture by the Co^{2+}/Co^{3+} redox shuttles for the YD2-o-C8–sensitized nanocrystalline TiO_2 films exhibits very high V_{oc}. By introducing a complementary absorption spectrum to YD2-o-C8, this co-sensitized nanocrystalline TiO_2 film showed an impressive panchromatic photocurrent response in the visible range and the more than 90% of IPCE was recorded in a large wavelength domain below 700 nm.

However, Pt has disadvantages due to its high cost and limited availability. Additionally, Pt can dissolve in the I^-/I_3^- redox shuttle electrolyte solution to produce some species, such as PtI_4.[37] Although Pt is very effective for catalyzing I_3^- reduction, it is less effective in the Co-based redox system.[7, 38] On the other hand, because the Co^{2+}/Co^{3+} redox shuttles contain various ligands that can influence the electrochemical characteristics, the use of Pt in Co-mediated DSSCs remains controversial.[10, 24] In this context, low cost Pt-free materials, such as carbon materials, TMCs, conductive polymers, and hybrids have been proposed to replace the Pt catalysts. The detailed photovoltaic parameters of Co-mediated DSSCs with various

CEs and dyes are summarized in **Table 1**.

Table 1. Photovoltaic parameters of Co-mediated DSSCs with various CEs and dyes (AM 1.5, 100 mW cm^{-2})

CEs	J_{sc} (mA cm^{-2})	V_{oc} (mV)	FF	PCE (%)	Area (cm^2)	Dye	Electrolyte	*Refs.*
Pt	17.66	935	0.74	12.3	0.36	Y123/YD2–o–C8	$[Co(bpy)_3]^{2+/3+}$	36
Pt	7.6	840	0.59	3.8	0.40	D35	$[Co(dtb)_3]^{2+/3+}$	39
Pt	7.7	830	0.64	4.1	0.40	D35	$[Co(dtb)_3]^{2+/3+}$	39
Pt	7.23	650	0.62	2.91	--	--	$[Co(dtb)_3]^{2+/3+}$	12
Pt	15.2	910	0.66	9.0	0.20	Y123	$[Co(bpy)_3]^{2+/3+}$	34
Pt	13.38	828	0.685	7.59	0.25	FNE29	$[Co(bpy)_3]^{2+/3+}$	40
Pt	8.55	800	0.66	4.49	0.64	YD2-o-C8	$[Co(bpy)_3]^{2+/3+}$	41
Pt	15.09	780	0.70	8.24	0.25	FNE29	Co^{2+}/Co^{3+}	42
Pt	0.87	320	0.4	0.7	0.50	--	$[Co(dtb)_3]^{2+/3+}/[Fe(dmb)_3]^{2+/3+}$	43
Pt	11.8	885	0.72	7.5	0.25	LEG4	$[Co(bpy)_3]^{2+/3+}/I^-/I_3^-$	44
SWCNT	7.4	800	0.62	3.6	0.40	D35	$[Co(bpy)_3]^{2+/3+}$	39
C_a	8.38	630	0.65	3.43	--	N719	$[Co(dtb)_3]^{2+/3+}$	12
OMC	9.59	640	0.66	4.05	--	N719	$[Co(dtb)_3]^{2+/3+}$	12
GNP	18.1	910	0.78	13	0.28	SM315	$[Co(bpy)_3]^{2+/3+}$	20
GNP	12.7	1030	0.70	9.3	0.20	Y123	$[Co(bpy)_3]^{2+/3+}$	45
GNP	14.8	878	0.72	9.4	0.10	Y123	$[Co(bpy)_3]^{2+/3+}$	35
GO-HT	15.2	898	0.65	8.8	0.20	Y123	$[Co(bpy)_3]^{2+/3+}$	34
RGO	15.6	891	0.61	8.4	0.20	Y123	$[Co(bpy)_3]^{2+/3+}$	34
FGS	8.49	813	0.65	4.51	0.25	D35	$[Co(bpy)_3]^{2+/3+}$	46
Printed-C	5.6	540	0.39	1.2	0.10	Z907	Co^{2+}/Co^{3+}	47
TiC	9.77	640	0.66	4.13	--	N719	$[Co(dtb)_3]^{2+/3+}$	12
NbO_2	9.14	610	0.65	3.62	--	N719	$[Co(dtb)_3]^{2+/3+}$	12
Ta_3N_5	11.69	783	0.32	2.89	0.25	FNE29	$[Co(bpy)_3]^{2+/3+}$	40
TaON	11.35	773	0.29	2.54	0.25	FNE29	$[Co(bpy)_3]^{2+/3+}$	48
$Co_{0.85}Se$	7.37	443	0.45	1.57	--	N907	Co^{2+}/Co^{3+}	49
CoS	12.84	805	0.65	6.72	0.159	C218	$[Co(bpy)_3]^{2+/3+}$	50
$W–O_V–W$	9.26	800	0.67	4.85	0.64	YD2-o-C8	$[Co(bpy)_3]^{2+/3+}$	41
W–O–W	8.89	810	0.65	4.49	0.64	YD2-o-C8	$[Co(bpy)_3]^{2+/3+}$	41
PEDOT	15.9	910	0.71	10.30	0.20	Y123	$[Co(bpy)_3]^{2+/3+}$	51
PEDOT	10.7	865	0.70	6.3	0.25	LEG4	$[Co(bpy)_3]^{2+/3+}$	52
PEDOT	12.15	1027	0.69	8.62	0.20	Y123	$[Co(bpy)_3]^{2+/3+}$	29
PProDOT1	12.62	999	0.78	9.9	0.20	Y123	$[Co(bpy)_3]^{2+/3+}$	29
PProDOT2	11.95	1003	0.73	8.7	0.20	Y123	$[Co(bpy)_3]^{2+/3+}$	29
PProDOT-Et_2	11.51	1006	0.70	8.0	0.20	Y123	$[Co(bpy)_3]^{2+/3+}$	29
PProDOT-Me_2	12.33	1006	0.70	8.74	0.20	Y123	$[Co(bpy)_3]^{2+/3+}$	29
PProDOT	13.06	998	0.77	10.08	0.20	Y123	$[Co(bpy)_3]^{2+/3+}$	23
PANI1	15.09	780	0.70	8.24	0.25	FNE29	$[Co(bpy)_3]^{2+/3+}$	42
PANI2	12.76	720	0.65	5.97	0.25	FNE29	$[Co(bpy)_3]^{2+/3+}$	42
GO/GNP	15.6	885	0.67	9.3	0.20	Y123	$[Co(bpy)_3]^{2+/3+}$	34
C/GNP	14.3	865	0.74	9.11	0.20	Y123	$[Co(bpy)_3]^{2+/3+}$	53
AgNW/GNP	6.45	550	0.52	1.61	0.25	N719	Co^{2+}/Co^{3+}	54
RGO/Ta_3N_5	13.53	837	0.69	7.85	0.25	FNE29	$[Co(bpy)_3]^{2+/3+}$	40
RGO/TaON	13.38	829	0.69	7.65	0.25	FNE29	$[Co(bpy)_3]^{2+/3+}$	48
TiN/PEDOT	13.21	840	0.75	8.26	0.16	--	$[Co(bpy)_3]^{2+/3+}$	55
TiC/PEDOT	12.68	838	0.76	8.09	0.16	--	$[Co(bpy)_3]^{2+/3+}$	55
$Co_{0.85}Se/Ni_{0.85}Se$	7.37	651	0.53	2.54	--	N907	Co^{2+}/Co^{3+}	49

3.2 Carbon materials

Due to the good chemical stability, electrical conductivity and catalytic activity of carbon materials, they were ideal candidates for replacing Pt in DSSCs. As early as 1996, graphite and carbon black (C_b) were used as the CEs materials in the I^-/I_3^- redox system and obtained a PCE of 6.7%.[56] Meanwhile, carbon materials used in Co-mediated DSSCs can exhibit more excellent performance. The ordered

mesoporous carbon and active carbon (C_a) were investigated as CEs materials, and achieved PCEs of 4.05% and 3.43%, respectively.[12] In addition, because of their high conductivity, good catalytic functions and excellent flexibility, the single-walled carbon nanotube (SWCNT) CEs in Co-mediated DSSCs achieved excellent performance.[39] By comparing of the *J-V* curves with different CEs in **Fig. 5** for the Co^{2+}/Co^{3+} redox shuttles electrolyte solution, it can be seen that the PCE of the SWCNT plastic CE was 3.6%, which is close to the PCE of DSSCs with sputtered Pt on indium tin oxide-plain polyethylene terephthalate (ITO/PET) (3.8%).

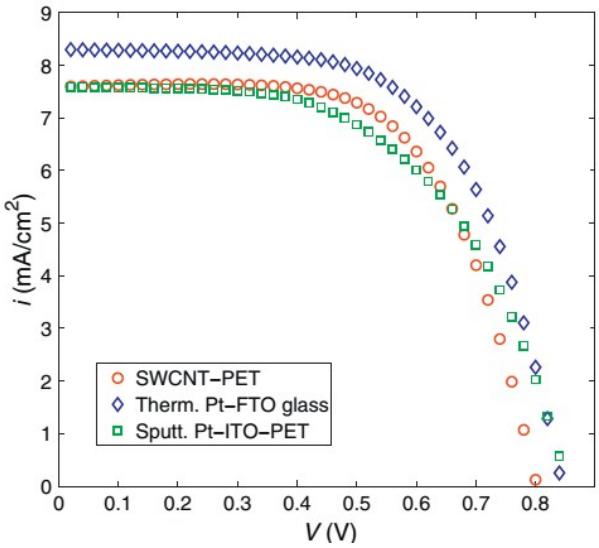

Fig. 5. *J-V* curves of the Co-mediated DSSCs with the different CEs. Reprinted with permission from ref.[39] Copyright 2013, Elsevier.

Graphene nanoplatelet (GNP) is a very promising alternative CE material. Recently, an FTO-supported GNP CE was synthesized to be active for the $Co(bpy)_3^{2+/3+}$ redox shuttles with a molecularly engineered porphyrin sensitizer (SM315), and achieved a maximum PCE of 13.0%.[20] Compared to the green sensitizer (SM371), the sensitizer SM315 achieved the high IPCE value of 80% in the wavelength range from 450 nm to 750 nm in **Fig. 6**(**a**), implying higher light capture efficiency of DSSCs. **Figure 6**(**b**)

shows the *J-V* curve of DSSCs with dyes SM371 and SM315. Although the V_{oc} of 0.91 V was slightly lower, the device with sensitizer SM315 attained a higher J_{sc} (18.1 mA cm^{-2}) and PCE of 13.0%, thereby outperforming SM371 as a result of the improvement in visible and near-infrared light harvesting.

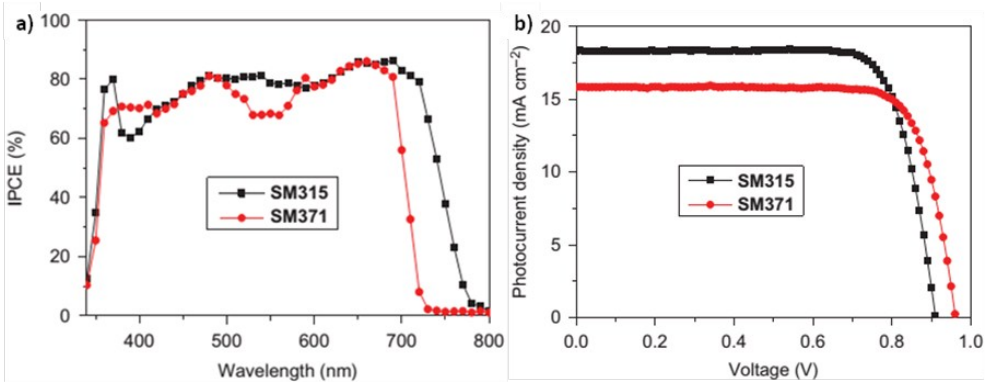

Fig. 6. a) photocurrent action spectrum for SM371 (red) and SM315 (black), and b) *J-V* curve of DSSCs under AM 1.5, 100 mW cm^{-2}. Reprinted with permission from ref.[20] Copyright 2014, Nature.

Meanwhile, GNP could outperform Pt for Co-mediated DSSCs both in R_{ct} and in electrochemical stability.[34-35, 45, 57] The *J-V* curves of Co(bpy)$_3$-mediated DSSCs with GNP-FTO and Pt-FTO CEs are shown in **Fig. 7**(**a**). At higher illumination intensity, the GNP-FTO CE exhibited superior electrocatalytic activity and PCE compared to the Pt-FTO CE. Values of 878 mV, 14.8 mA cm^{-2}, 0.72, and 9.4% have been achieved for V_{oc}, J_{sc}, *FF*, and PCE, respectively (see **Table 1**). **Figure 7**(**b**) shows *J-V* characteristics of DSSCs using GNP-FTO CEs based on Co(L)$_2$ redox shuttles, where L is 6-(1H-pyrazol-1-yl)-2,2'-bipyridine, under various simulated solar irradiation conditions. Interestingly, the investigation for Co-mediated systems shows that the dark current near V_{oc} is always enhanced compared with that of the GNP-FTO CE. A possible reason for this is that the dark current is not controlled by the electron flow at

the CE, but by the electrons flow from the nanocrystalline TiO_2 film into the redox electrolyte solution.

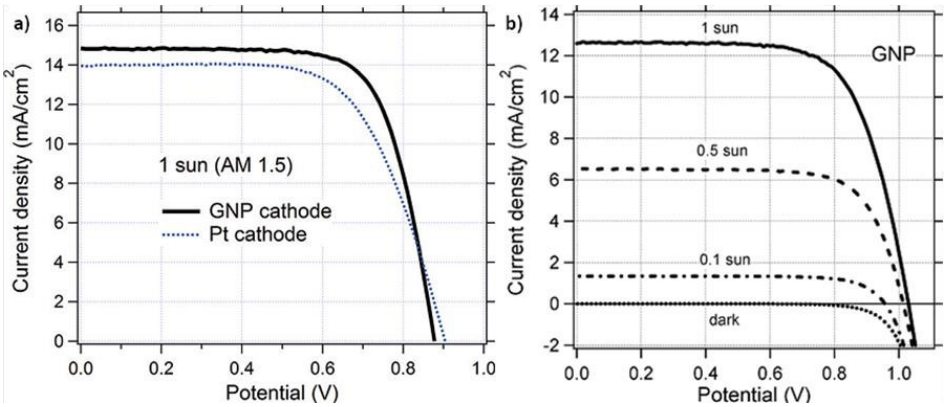

Fig. 7. a) *J-V* characteristics of DSSC with different CEs. Reprinted with permission from ref.[35] Copyright 2011, American Chemical Society. b) *J-V* characteristics of GNP CE under the different illumination intensity. Reprinted with permission from ref.[45] Copyright 2011, American Chemical Society.

Functionalized graphene sheet (FGS) has a large surface area like other carbon materials, and the FGS has lattice defects and oxygen-containing functional groups, which are favorable characteristics for replacing Pt as a catalyst.[46, 58-60] The new synthetic FGS with high surface area was used as a CE for Co-mediated DSSCs. In view of the photovoltaic performance and EIS fitting data, the R_{ct} of the CEs is a major factor for the performance of DSSCs. The impedance results for FGS CE using different electrolyte solution with I-, Co-, and S-based mediators are summarized in **Fig. 8**(**a**). The FGS CE employing Co^{2+}/Co^{3+} redox shuttles showed lower effective R_{ct} (<1 Ω cm^2), exhibiting higher catalytic activity for Co^{2+}/Co^{3+} reduction. The *J-V* curves of DSSCs using the two types of CEs, seen in **Fig. 8**(**b**), showed that FGS CE perform better than the platinized electrode.

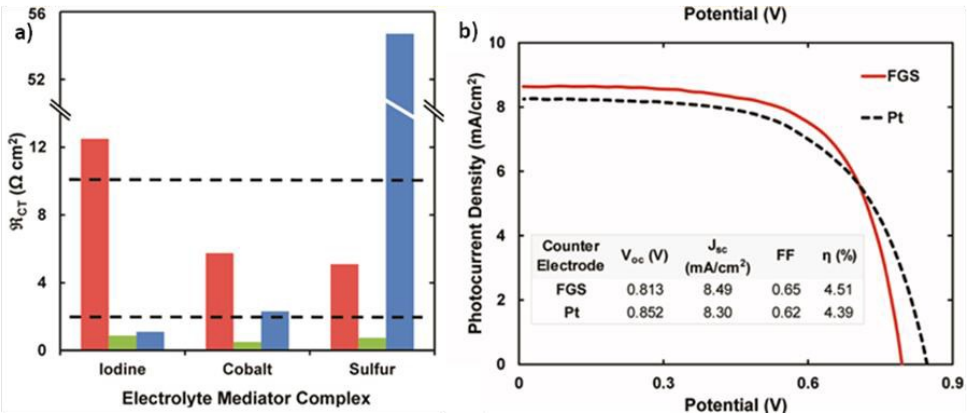

Fig. 8. a) Comparison of R_{ct} for FGS CE using acetonitrile electrolyte solution with I-, Co-, and S-based mediators. Red: FGS CEs from previous work[61]. Green: FGS CEs. Blue: Thermally decomposed chloroplatinic acid electrodes. b) *J-V* curve characteristics of DSSCs using thermally decomposed chloroplatinic acid (Pt) and FGS CEs based on Co-mediated DSSCs. Reprinted with permission from ref.[46] Copyright 2012, American Chemical Society.

L. Kavan et al. reported that graphene oxide after heat treatment at 450 °C in Ar atmosphere (GO-HT) and reduction graphene oxide (RGO) achieve better mechanical and electrochemical stability than pure graphene nanoplatelet. The PCEs of GO-HT and RGO were 8.8% and 8.4%, respectively.[34, 57] The parameters of the GO-HT CE are promising from the *J-V* characteristics of GO-HT CE for DSSCs, as seen in **Fig. 9**. The corresponding R_{ct} value of GO-HT (0.51 Ω cm^2) was smaller than that of RGO (3.4 Ω cm^2). It is likely that electrocatalytic activity of GO-HT and RGO is correlated with the density of dangling bonds, step edges, and other sharp atomic features, but this requires further investigation.

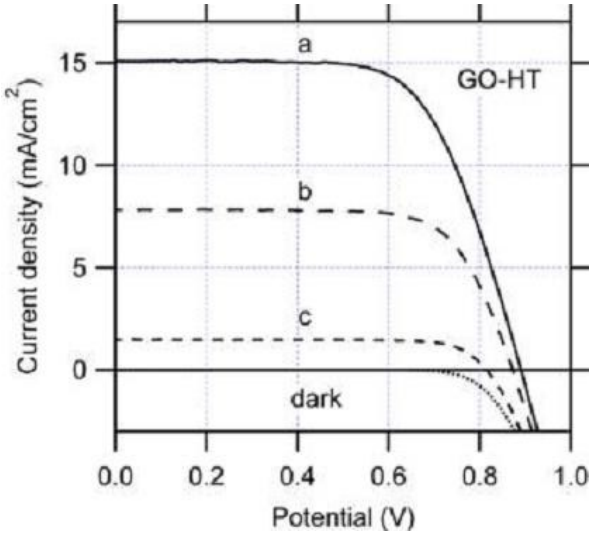

Fig. 9. *J-V* characteristics of DSSCs assembled with GO-HT CE and Y-123 sensitized TiO_2 photoanode in acetonitrile solution of Co^{2+}/Co^{3+}. Reprinted with permission from ref.[34] Copyright 2012, American Chemical Society.

The shortcomings of carbon materials, such as opacity and poor adhesion between the carbon film and the substrate, limited their practical applications. The poor mechanical stability for traditional carbon CEs was unfavorable for long-term use. Through the introduction of graphene oxide as a surfactant in a recent study, the adhesion between the GNP film and the substrate was shown to be significantly enhanced.[24, 34]

3.3 Transition metal compounds (TMCs)

Recently, TMCs exhibiting Pt-like catalytic behavior have attracted considerable attention due to their low cost, high electrocatalytic activity, and stability.[62-63] Ma et al. investigated TMCs, such as oxides, carbides, nitrides of some elements including Ti, W, Nb, Cr, V, Mo and Zr, and sulphides (WS_2 and MoS_2), as CE materials in DSSCs.[2, 64-65] Meanwhile, our group have also studied TMCs such as HfO_2, TaO, Ta_2O_5, SiC, Ta_4C_3, Ta_3N_5, TaO/MC (MC=mesoporous carbon), TaC/MC, HfO_2/MGC (MGC represents mesoporous graphitic carbon), HfO_2/C, $Hf_7O_8N_4/HfO_2$/C and

Pt/SiC.[24, 66-72] In the I^-/I_3^- system, NbO_2, WO_2, and TaO exhibited outstanding performance and achieved higher PCEs of 7.88%, 7.25%, and 6.48%, respectively. Recently, researchers have begun to focus on NbO_2 and TiC as CEs for Co-mediated DSSCs.[12] As shown in the **Fig. 10**, the DSSCs with TiC CE showed V_{oc}, J_{sc}, *FF* and PCE of 640 mV, 9.77 mA cm^{-2}, 0.66, and 4.13% respectively. Compared with platinized electrode, the TiC CE showed a smaller R_{ct} of 0.7 Ω cm^2, which is mainly due to the larger surface area of TiC CE which provides more catalytic sites for Co^{3+} ion reduction. Furthermore, the NbO_2 CE exhibited the same characteristics as the TiC CE with the former achieving values for V_{oc}, J_{sc} and *FF* of 0.61 V, 9.14 mA cm^{-2}, and 0.65, respectively. It seems from **Table 1** that TMCs cannot match as well with Co-mediated redox shuttles as with I-mediated redox shuttle.

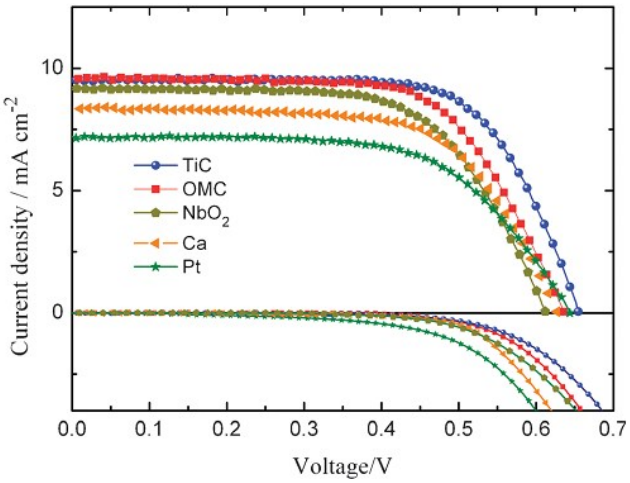

Fig. 10. *J-V* curves of the DSSCs based on Pt-free and Pt CEs. Reprinted with permission from ref.[12] Copyright 2012, Royal Society of Chemistry.

Ta_3N_5, TaON, $Co_{0.85}Se$ and CoS were also used as alternative to Pt in conjunction with Co^{2+}/Co^{3+} redox shuttles.[40, 48-50] The Ta_3N_5 nanorods have a relatively high crystallinity, shown in **Fig. 11**(**a**). The drop-casted Ta_3N_5 films on FTO substrates, **Fig. 11**(**b**), showed that the surface of the Ta_3N_5 nanorods film has a rich internal porous

structure, which provides more catalytic sites for the reduction of Co^{3+} ion. However, compared with the *FF* (0.685) of Pt, the lower *FF* (0.316) of Ta_3N_5 nanorods led to the lower PCE of 2.89%. In addition, due to Ta^{5+} exhibiting noble-metal-like electron features, the Ta_3N_5 showed similar performance to a typical platinized electrode. Thus, the TaON, having similar properties with Ta_3N_5, obtained lower PCE of 2.54%.

In conjunction with the high absorption coefficient of organic dye (C218), CoS CE can be used as a promising alternative to platinized electrode for DSSCs based on the Co^{2+}/Co^{3+} redox shuttles. The SEM image of CoS showed a honeycomb-like surface structure with better interconnectivity as seen in **Fig. 11**(**c**). This structure led to a J_{sc} of 12.84 mA cm^{-2}, a V_{oc} of 805 mV and a PCE of 6.72%. The PCE of CoS CE was comparable to the performance of the platinized electrode (6.94%). In addition, bimetallic alloy also can be used as alternative to platinized electrode. The $Co_{0.85}Se$, with a highly uniform honeycomb-like structure (**Fig. 11**(**d**)) provided a greater surface area and more catalytic sites; however, a PCE of only 1.57% was obtained, which indicated that the photovoltaic performance of DSSCs using $Co_{0.85}Se$ CEs requires further improvement.

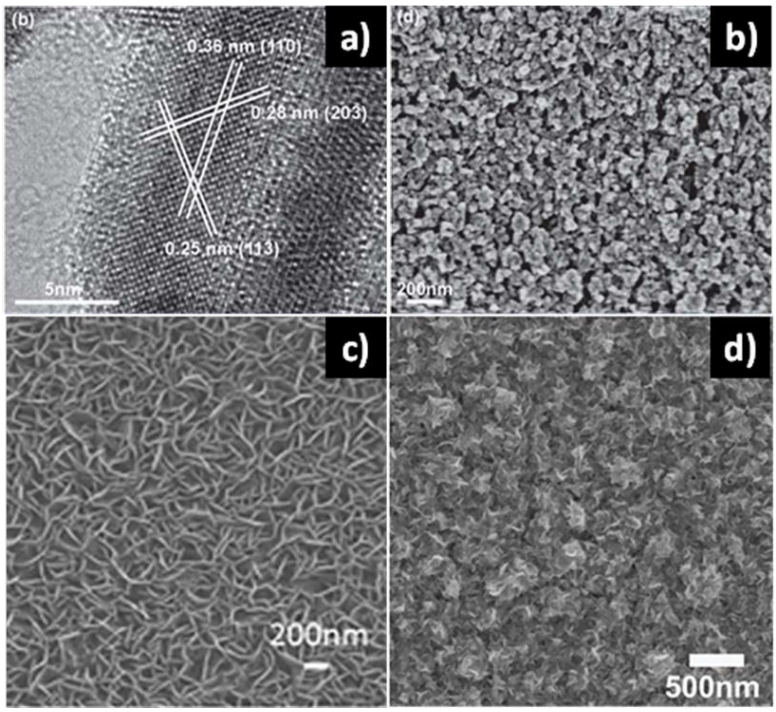

Fig. 11. a) HRTEM image of Ta_3N_5 nanorods. Reprinted with permission from ref.[40] Copyright 2013, Royal Society of Chemistry. b) Top-view SEM image of Ta_3N_5 CEs. Reprinted with permission from ref.[40] Copyright 2013, Royal Society of Chemistry. c) SEM image of CoS CEs. Reprinted with permission from ref.[50] Copyright 2015, Elsevier. d) SEM image of $Co_{0.85}Se$. Reprinted with permission from ref.[49] Copyright 2014, Wiley.

Tungsten oxides with notable catalytic properties are efficient catalysts in DSSCs for Co^{2+}/Co^{3+} redox shuttles. In particular, the electrocatalytic properties of $W_{18}O_{49}$ with surface oxygen vacancies (W-O_V-W) were investigated.[41] SEM images of W-O_V-W and schematic surface oxygen vacancies filling on $W_{18}O_{49}$ (W-O-W) are shown in **Fig. 12**(**a-b**). The W-O_V-W exhibited a richly porous and loose structure, which allowed the electrolyte solution to fill the pores and played a crucial role in the catalytic reactions. The *J-V* curves obtained for these DSSCs based on W-O_V-W, W-O-W and platinized electrodes, are shown in **Fig. 12**(**c**). It is clear that the catalytic performance of CEs comprised of $W_{18}O_{49}$ nanowires for Co-mediated DSSCs have a comparable performance to that of platinized electrode.

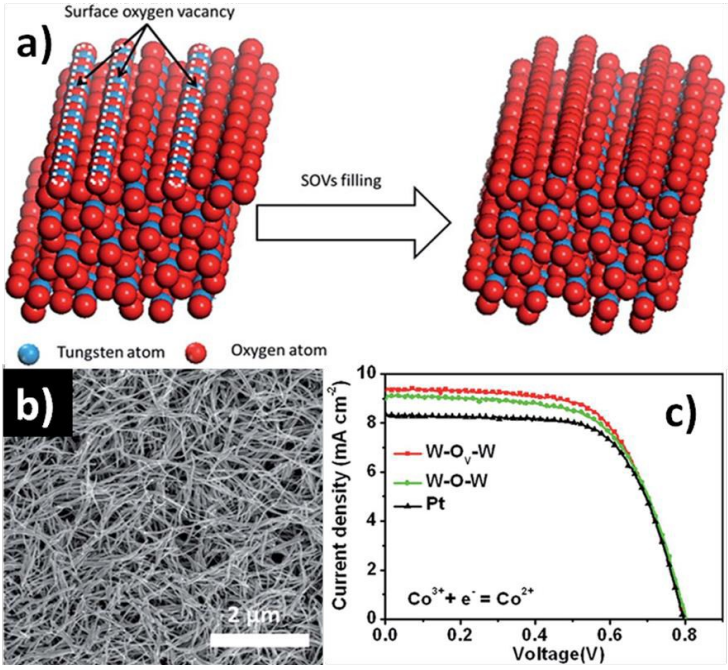

Fig. 12. (a) Schematic surface oxygen vacancies (SOVs) filling on $W_{18}O_{49}$. (b) SEM image of W-O_V-W (c) *J-V* curves of DSSCs utilizing three different catalytic electrodes for Co^{2+}/Co^{3+} redox shuttles. Reprinted with permission from ref.[41] Copyright 2014, Royal Society of Chemistry.

Most of the TMCs materials exhibited Pt-like catalytic activity; however, the synthesis procedures of TMCs do not allow for the control of the morphology, which limits the commercial applications of DSSCs going forward.

3.4 Conductive polymer

Compared with other materials, conductive polymers have unique properties of transparency and flexibility, and as result they can be developed into flexible and transparent electrodes. In addition, conductive polymers have several others advantages such as low cost, good conductivity, and high catalytic activity.[15] In the recent past, based on these characteristics, conducting polymers, such as poly(3,4-ethylenedioxythiophene) (PEDOT), polyaniline (PANI) and poly(3,4-propylenedioxythiophene) (PProDOT), as alternative CEs have been applied in Co-mediated DSSCs. A PProDOT layer with high surface area was reported.[23] The

notable lower R_{ct} of 2.5 Ω cm^2 significantly improved the *FF* (0.77), hence a higher PCE of 10.08% was obtained.

Meanwhile, the implementation of PEDOT in Co-mediated DSSCs systems has attracted the interest of researchers. M. Grätzel et al. used PEDOT as a CE in DSSCs based on two Co^{2+}/Co^{3+} redox shuttles, namely Co^{2+}/Co^{3+} tris(2,2'-bipyridine) ($Co(bpy)_3$) and Co^{2+}/Co^{3+} tris(1,1'-phenanthroline) ($Co(phen)_3$).[51] The porous morphology of the PEDOT layer, seen in **Fig.13**(**a**), reduced the diffusion distance of electrolyte solution, which resulted in a decrease of R_{ct} and better Co^{3+} ion reduction. The *J-V* characteristics of DSSCs based on the PEDOT films and platinized electrodes for two Co-based redox shuttles are shown in **Fig. 13**(**b**), in which the Co-mediated DSSCs with PEDOT CE achieved significant values for V_{oc}, J_{sc}, *FF*, and PCE of 910 mV, 15.9 mA cm^{-2}, 0.71, and 10.3%, respectively. The improved *FF* for both electrolyte solution suggests a lower R_{ct} of the PEDOT film, attributed to its high surface area. In addition, the decrease of R_{ct} resulted in an increase of J_{sc}, thus achieving a competitive PCE.

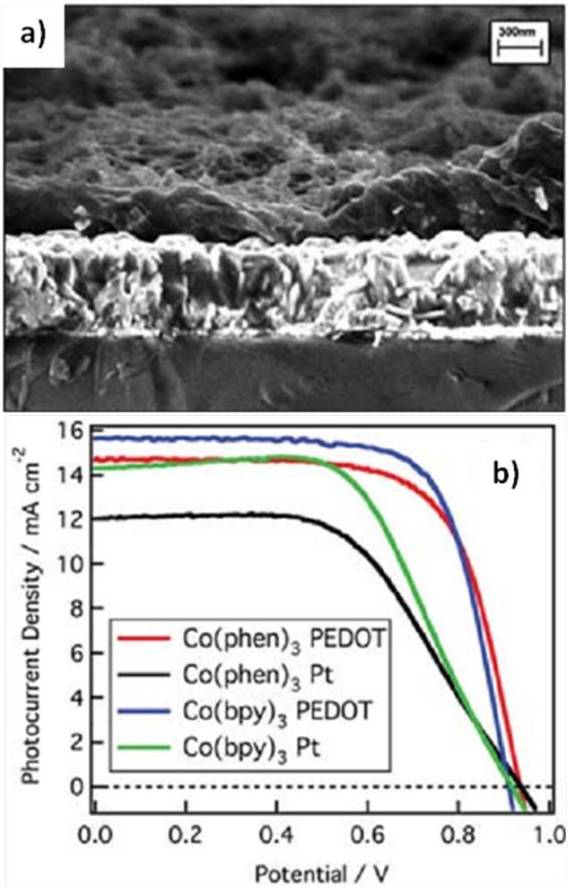

Fig. 13. a) SEM images of the crosssectional porous PEDOT film (top layer) on FTO coated glass. b) *J-V* response of Co(bpy)$_3$ and Co(phen)$_3$ based DSSCs using Pt and PEDOT CEs. Reprinted with permission from ref.[51] Copyright 2011, Royal Society of Chemistry.

PEDOT as such is an insoluble polymer. Thus to make its solution processable, the commercial product polystyrenesulfonate doped poly(3,4-ethylenedioxythiophene) (PEDOT: PSS) is used. However, PEDOT:PSS is an aqueous dispersion and has some drawbacks. One possibility for obtaining PEDOT is the electrodeposition of EDOT, which will also allow for the deposition of uniform film directly onto any conductive substrate, including FTO substrates. Varying thicknesses of PEDOT were used as CEs in Co-mediated DSSCs employing an organic dye (LEG4).[52] As illustrated in **Fig.14**(**a**), the *J-V* curves of the Co-mediated DSSCs with three different thicknesses CE materials were presented; the thinnest PEDOT layer of 270 nm attained the

highest PCE of 6.3%. The values of V_{oc}, J_{sc} and *FF* were 865 mV, 10.7 mA cm^{-2}, and 0.70, respectively. Higher PCE value of DSSCs with PEDOT CEs can be attributed to the higher *FF* and much lower R_{ct} (0.2 Ω cm^2) as compared with platinized electrode (5.3%). Meanwhile, the PEDOT CEs with lower series resistance (R_s), compared to the platinized electrode, indicated that the PEDOT CEs have better conductive charge transfer properties in the DSSCs. The SEM images of the PEDOT samples (270 nm) are shown in **Fig. 14b**. The high-surface area of the PEDOT films with an open mesoporous structure will lead to an increase in the catalytic activity.

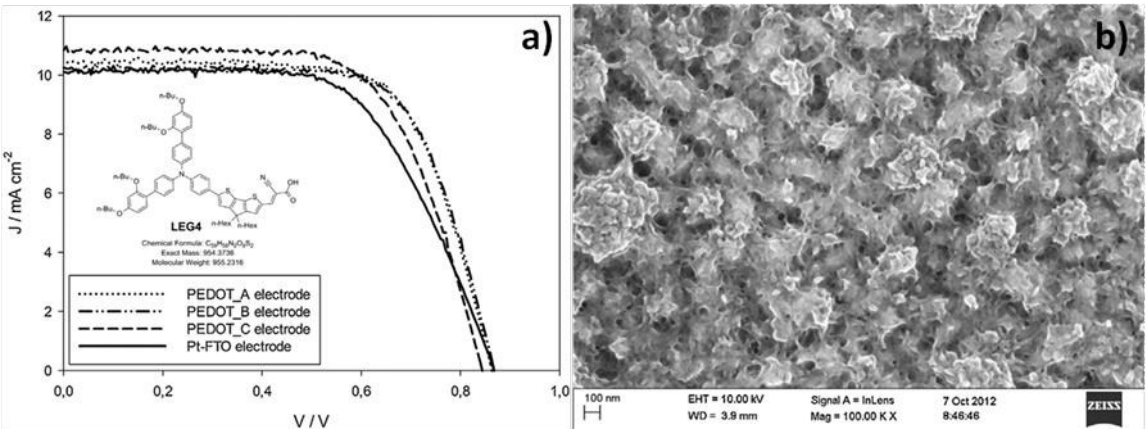

Fig. 14. a) *J-V* curves at 1 sun of the solar cells with different CEs. Insert: the molecular structure of the LEG4 dye. b) top-view SEM image of PEDOT films (270 nm) on FTO substrates.. Reprinted with permission from ref.[52] Copyright 2013, Elsevier.

The PEDOT and other polymers are used for CEs films in DSSCs assembled with $[Co(bpy\text{-}pz)_2](PF_6)_2$ and $[Co(bpy\text{-}pz)_2](PF_6)_3$ redox shuttles, in which the PEDOT film obtained significant PCE values as high as 8.26%.[29] The high performance of PEDOT-based CEs was attributed to a perfect match between the oxidation potential of the dye and the redox shuttle. The chemical structures of the monomer used can be seen in **Fig. 15**(**a**). The SEM image of PProDOT synthesized in an ionic liquid 1-butyl-3-methylimidazolium bis(trifluoromethylsulfonyl)imide (BMITFSI)

illustrates the compact granular porous structures with high surface areas (**Fig. 15**(**b**)), which are desired qualities for electrocatalysis and produce significant benefits for Co^{3+} ion reduction. Under the same conditions, compared with platinized electrodes, the photovoltaic performances of Co-mediated DSSCs with PProDOT using the $[Co(bpy\text{-}pz)_2](PF_6)_2$ and $[Co(bpy\text{-}pz)_2](PF_6)_3$ redox shuttles showed remarkable values of J_{sc}, V_{oc}, *FF*, and PCE which were 12.6 mA cm^{-2}, 1000 mV, 0.78, and 9.9%, respectively. The PProDOT film achieved broad IPCE values at 450 nm-650 nm (**Fig. 15**(**c**)). In all of the Co^{2+}/Co^{3+} redox shuttles, the PProDOT film exhibited enhanced V_{oc} over platinized electrodes. Moreover, PProDOT synthesized in the ionic liquids 1-ethyl-3-methylimidazolium tris(pentafluoroethyl) trifluorophosphate (EMIFAP), 3,4-(2',2'-dimethylpropylene)-dioxythiophene (Me_2-PProDOT) and 3,4-(2',2'-diethylpropylene)-dioxythiophene (Et_2-PProDOT) were also been investigated and achieved prominent PCEs of 8.7%, 8.74%, 8.0%, respectively, in the Co^{2+}/Co^{3+} redox shuttles system (**Table 1**).

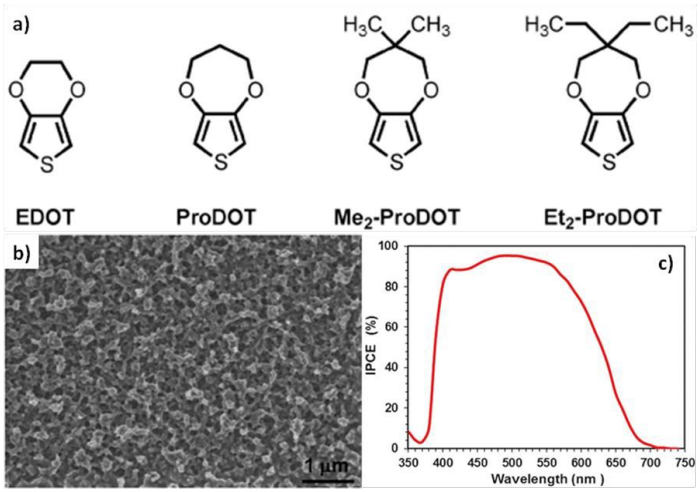

Fig. 15. (a) Molecular structures of the different compounds used as monomers for polymerization (b) SEM image of PProDOT (c) IPCE as function of wavelength of monochromatic light for PProDOT based CEs by using $[Co(bpy\text{-}pz)_2](PF_6)_2$ and $[Co(bpy\text{-}pz)_2](PF_6)_3$ as redox shuttles. Reprinted with permission from ref.[29] Copyright 2012, Royal Society of Chemistry.

The oriented PANI nanowire prepared by in situ growth was interesting and has been investigated as a CE in Co-mediated DSSCs.[42] The oriented PANI nanowire CE showed high uniformity and achieved a PCE of 8.24%, which was higher than that obtained by either a drop-cast PANI (5.97%) having a random network-like structure (**Fig. 16**(**a**)) or platinized electrode (6.78%) under the same conditions. Compared with the PANI random network and Pt, the lowest R_{ct} of the PANI nanowire represents the most excellent catalytic performance. The *J*-*V* curves of Co-mediated DSSCs with PANI nanowires and PANI random network are shown in **Fig. 16**(**b**). The significant values of V_{oc}, J_{sc}, *FF*, and PCE for PANI nanowire CE were 780 mV, 15.09 mA cm^{-2}, 0.7, and 8.24%, respectively. Meanwhile, the PANI nanowire CE showed higher IPCE values (**Fig. 16**(**c**)), and the maximum IPCE of 87% was obtained at 440 nm. The PANI-based nanowire was found to be a good alternative material to replace the expensive Pt as the CE of DSSCs.

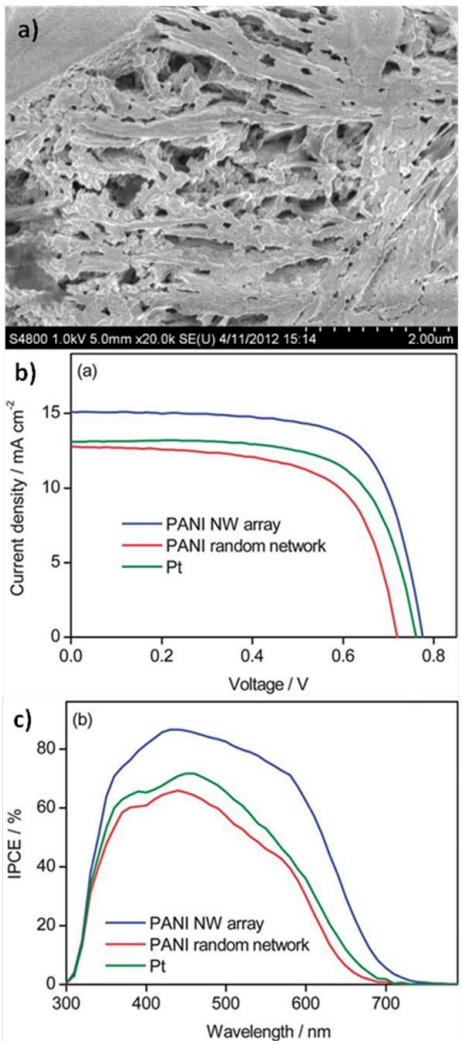

Fig. 16. a) FESEM image of the drop-casted PANI film. b) *J-V* characteristics and c) IPCE spectra of DSSCs based on the PANI nanowire, drop-cast PANI film and Pt CEs, respectively. Reprinted with permission from ref.[42] Copyright 2013, Royal Society of Chemistry.

Although the performance of DSSCs using conducting polymer CEs is impressive, complex fabrication and poor stability of these polymer CEs have limited their practical application.

3.5 Hybrids

Hybrid CEs in DSSCs have become increasingly popular due to the synergetic effects derived from the different components of the hybrids.[24] In other words, all of the excellent qualities of the component materials are combined into one material. Here, we will provide a summary of the hybrid CEs based on Co-mediated DSSCs.

Due to their large surface area and high conductivity, carbon materials were found to be excellent components for hybrid CEs. By optimizing the proportions between graphene oxide (GO) and GNP to improve their catalytic properties, Kavan et al. investigated hybrids of GO/GNP as CEs in DSSCs.[34] The catalytic activity of GNP-based materials is related to the amount of oxygen in the carbon skeleton. The optimized GONP50 (the amounts of GO, T_{550}=90%) CE showed the lowest R_{ct}, significantly enhancing its catalytic activity, and also had remarkable values of V_{oc}, J_{sc}, *FF*, and PCE of 885 mV, 15.6 mA cm^{-2}, 0.67, and 9.3%. Due to the intimate interaction of hydrophilic functionalities between GO and the FTO surface, the GO/GNP films have strong adhesion to the FTO substrate. Aside from GO, carbon was regarded as a component of hybrid CEs. A new type of carbon/graphene hybrid was reported as a CE material. Compared with the GNP films, the carbon/graphene hybrids presented enhanced catalytic performance and improved adhesion to the FTO substrate via a conductive carbon matrix, yielding significant values of V_{oc}, J_{sc}, *FF*, and PCE were 865 mV, 14.3 mA cm^{-2}, 0.74, and 9.11%, respectively.[53] The carbon/graphene used as CEs had lower R_{ct}, enhanced *FF*, and high PCE values for Co-mediated DSSCs as compared to platinized electrode. In addition, nanohybrids carbon/graphene showed an almost identical dark current compared to that of the Pt based CE, which may be associated with the improved adhesion of the catalyst particles.

Carbon material can be introduced into the hybrid CEs, along with metal material which is also a prominent component of hybrids. GNP loaded on the surface of silver

nanowire (Ag-NW) films can be used as a catalytic CE in Co-mediator DSSCs, and this combination resulted in a remarkable improvement of electrocatalytic properties.[54] The schematic diagram of Ag-NW and Ag-NW/GNP-based CEs and a cross-sectional tilted view of the Ag-NW/GNP film are shown in **Fig. 17**. The GNP layer provides a larger interfacial surface area with the Co^{2+}/Co^{3+} redox shuttles. Moreover, the Ag-NW/GNP showed a lower R_{ct} value of 11.57 Ω cm^2, indicating higher electrocatalytic activity than that of Ag-NW (47.73Ω cm^2). The values of V_{oc}, J_{sc}, and *FF* for the Ag-NW/GNP CEs were 550 mV, 6.45 mA cm^{-2}, and 0.52, respectively. The PCE of Ag-NW/GNP (1.61%) is lower than that of Pt (1.87%).

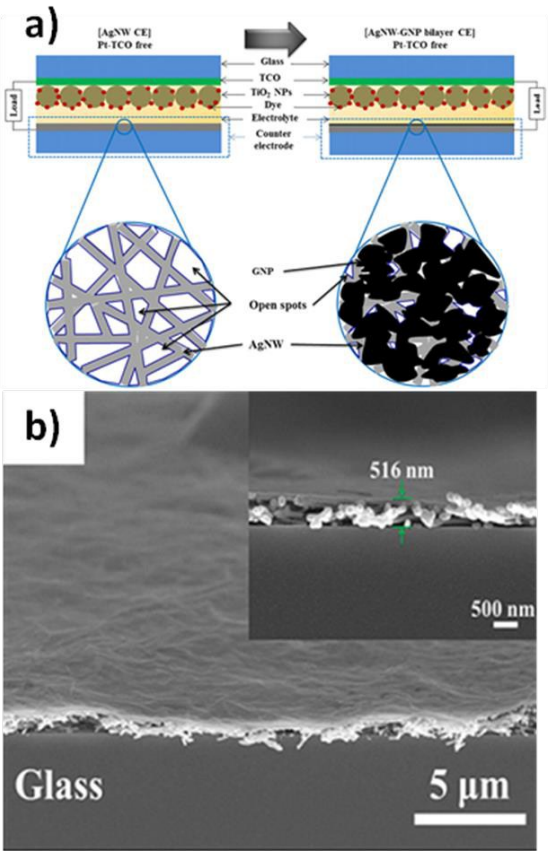

Fig. 17. (a) Schematic illustration of Ag-NW/GNP CEs and (b) cross-sectional tilted view Ag-NW/GNP CEs. Reprinted with permission from ref.[54] Copyright 2013, Elsevier.

The RGO/Ta_3N_5 hybrids, fabricated by mixing graphene oxide with

pre-synthesized Ta_3N_5 nanorods, were also used as CE materials in Co-mediated DSSCs. The SEM image of RGO/Ta_3N_5, as shown in **Fig 18**(**a**), shows Ta_3N_5 nanorods with a great deal of corrugation embedded into the RGO sheets. The specific surface areas of the RGO/Ta_3N_5 hybrids were 57.6 m^2 g^{-1}, higher than those of Ta_3N_5 (39.8 m^2 g^{-1}) and RGO (12.3 m^2 g^{-1}). The lattice surface defects of RGO are beneficial for improving the electrical performance. Meanwhile, the network structure of RGO is able to provide high electrical conductivity. With the synergetic catalytic effect of RGO and Ta_3N_5 nanorods, the RGO/Ta_3N_5 hybrids exhibited comparable electrocatalytic performance for the reduction of Co^{3+} and better electrocatalytic stability in Co^{2+}/Co^{3+} redox shuttles compared with Pt; the RGO/Ta_3N_5 hybrids were able to achieve the remarkable PCE of 7.85%.[40] The *J-V* curves of the DSSCs using RGO/Ta_3N_5, RGO, Ta_3N_5 nanorods, and Pt as CEs are shown in **Fig. 18**(**b**). It is obvious that all of the photovoltaic parameters based on RGO/Ta_3N_5 were higher than those of the DSSCs using RGO or Ta_3N_5 nanorods.

Interestingly, the hybrids of TaON nanoparticles embedded in the RGO sheets were also reported by their group.[48] **Figure 18**(**c**) shows the SEM images of the drop-casted RGO/TaON and RGO films and the electron-transport network structure of RGO/TaON nanohybrids, which can be advantageous for Co^{3+} ion reduction. Compared with RGO and TaON, the specific surface area of the RGO/TaON hybrids had higher values of 54.3 m^2 g^{-1}. The total current of the Co^{2+}/Co^{3+} redox shuttles reaction was increased, which led to higher values of J_{sc} and V_{oc}. The *J-V* curves of DSSCs using TaON, RGO, RGO/TaON and Pt as CEs are shown in **Fig. 18**(**d**) (also

see **Table 1**). The improved performances of the RGO/TaON hybrids resulted from the synergistic effect of RGO and TaON.

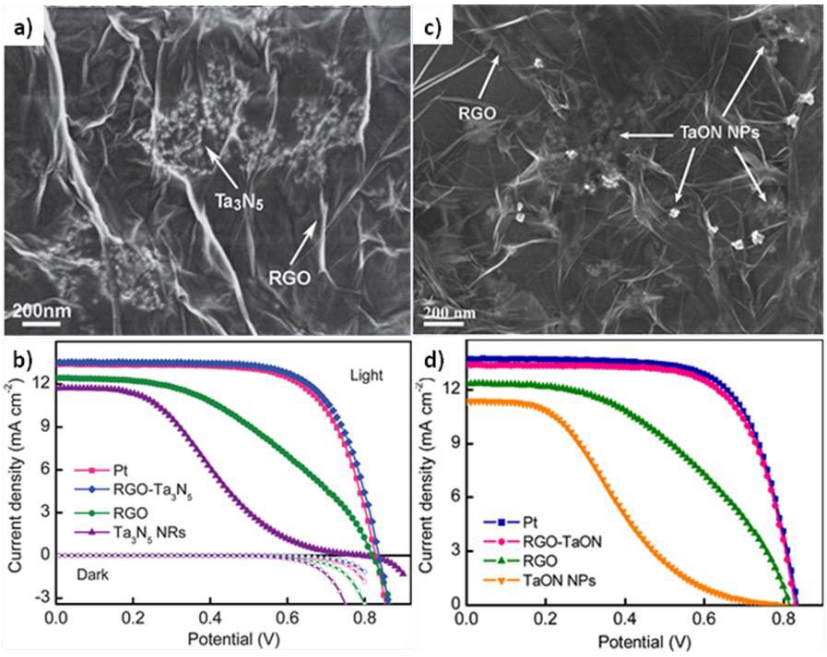

Fig. 18. (a) Top-view SEM images of RGO/Ta_3N_5. (b) *J-V* characteristics of DSSCs with different CEs of RGO/Ta_3N_5, RGO, Ta_3N_5 nanorods and Pt. Reprinted with permission from ref.[40] Copyright 2013, Royal Society of Chemistry. (c) Top-view SEM images of RGO/TaON. (d) *J-V* characteristics of DSSCs with different CEs of RGO/TaON, RGO, TaON nanorods and Pt. Reprinted with permission from ref.[48] Copyright 2013, American Chemical Society.

Furthermore, the hybrids of TMCs and conductive polymers can also be used as CEs for DSSCs. In a report, TiC/PEDOT and TiN/PEDOT nanohybrids synthesized by electrochemical deposition were developed as alternative catalysts in a Co-mediator system.[55] **Figure 19**(**a-b**) show SEM images of similar morphologies for two nanohybrids. The authors found that the PEDOT was distributed uniformly throughout the film and wraps firmly over the TiN particles. As a conductive binder, the PEDOT enhanced the adhesion between the nanoparticles and the substrate. The TiC and TiN layer provided a porous structure for the PEDOT to increase its active surface area. Based on the *J-V* curves of the Co-mediated DSSCs of the different CEs

(**Fig. 19**(**c**)), the photovoltaic performance of two nanohybrids outperformed that of Pt. The platinized electrode achieved a V_{oc} of 877 mV, a J_{sc} of 11.26 mA cm^{-2}, a *FF* of 0.75, and a PCE of 7.51%. For the TiN/PEDOT CE, excellent performance was observed with V_{oc}, J_{sc}, *FF*, and PCE values of 840 mV, 13.21 mA cm^{-2}, 0.75 and 8.26%, respectively. Meanwhile, the TiC/PEDOT CE also exhibited significant performance parameters values (**Table 1**). The higher J_{sc} of the hybrid CEs compared to that of plain PEDOT film is attributed to the larger active surface area of the hybrids. In addition, the R_{ct} values of two kinds of hybrids (< 1 Ω cm^2) indicated higher electrocatalytic activity than for Pt.

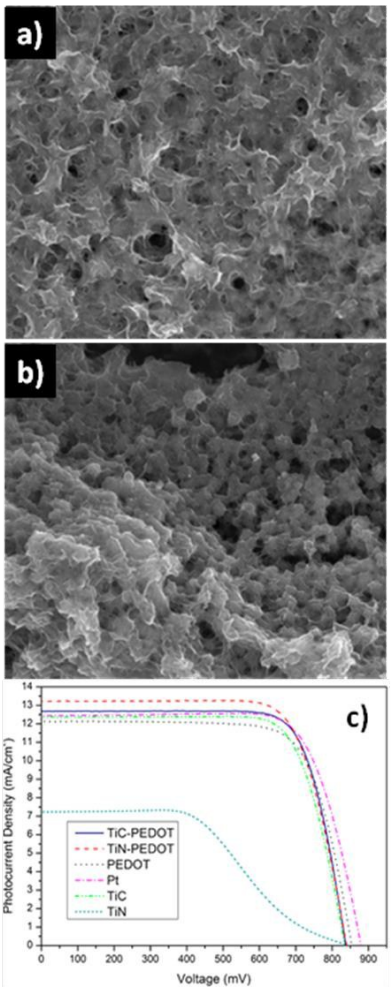

Fig. 19. SEM images of (a) TiC-PEDOT, (b) TiN-PEDOT and (c) *J-V* curves of DSSCs with various CEs. Reprinted with permission from ref.[55] Copyright 2014, American Chemical Society.

It is noted that the nanostructure hybrid catalysts with TMCs contribute to the Co^{3+} ion reduction reaction. In this context, $Co_{0.85}Se/Ni_{0.85}Se$ nanohybrid films were synthesized on FTO substrates.[49] As a result of the synergistic effects and the unique morphology of the $Co_{0.85}Se/Ni_{0.85}Se$ nanoparticles embedded with 2D nanoflakes, the Co-mediated DSSCs with $Co_{0.85}Se/Ni_{0.85}Se$ CE achieved a higher PCE of 2.54%: an improvement of 46% compared with the Pt (1.74%) under the same conditions. In addition, the $Co_{0.85}Se/Ni_{0.85}Se$ had much smaller R_{ct} value of 7.39 Ω cm^2, indicating higher electrocatalytic activity for the Co^{3+} reduction.

While hybrid materials as alternative CEs have many advantages, their poor adhesion to the conductive substrate limits their use in applications. Meanwhile, hybrid materials exhibit excellent performance in Co-mediated DSSCs due to the synergetic effects of them, nevertheless, the theory explanation is still unclear and some efforts should be paid in this field to improve applications of Co-mediated DSSCs.

4. Cobalt-based tandem-redox electrolyte solution

In 2010, to solve these problems of inefficient charge transfer and lower ion mobility for Co^{2+}/Co^{3+} redox shuttles, Caramori et al. investigated a novel tandem-redox electrolyte solution containing $[Co(dtb)_3]^{2+}/[Co(dtb)_3]^{3+}$ and $[Fe(dmb)_3]^{2+}/$ $[Fe(dmb)_3]^{3+}$, and demonstrated an improved electron-collection efficiency.[43] In a more recent study, DSSCs with an electrolyte solution including Co^{2+}/Co^{3+} redox shuttles and I^-/I_3^- redox shuttle were developed. In these interesting electrolyte solution, the Co^{2+}/Co^{3+} redox shuttles were responsible for the dye

regeneration and the I^-/I_3^- redox system participated in the reaction at the CE. With the cobalt-based redox system alone, the Pt CE obtained a J_{sc} of 11 mA cm^{-2}, a V_{oc} of 882 mV, a *FF* of 0.67 and a PCE of 6.5%. On the other hand, when used in conjunction with the tandem-redox electrolyte solution, the Pt CE had enhanced J_{sc}, V_{oc}, *FF*, and PCE of 11.8 mA cm^{-2}, 885 mV, 0.72, and 7.5%, respectively.[44] With the synergistic effects of the tandem-redox electrolyte solution, excellent DSSC performance can be obtained. This provides another important way to improve the performance of DSSCs.

5. Conclusions and outlook

In this mini-review, the recent progress and important contributions of CE materials, such as carbon materials, TMCs, conductive polymers, and hybrids, have been discussed and reviewed for Co-mediated DSSCs. These CEs are more suitable for the regeneration of the Co^{2+}/Co^{3+} redox shuttles, which is favorable for achieving high PCE. Due to the high surface area and high electrical conductivity, carbon materials were used in Co-mediated DSSCs, reaching a PCE of 13.0%. For TMCs, Pt-like catalytic behavior and good stability make them great potential alternatives to Pt. Because of transparency, flexibility and availability of conductive polymers, they used as CEs have made significant progress and a PCE of 10.30% was achieved in Co-mediated DSSCs. Moreover, hybrid CEs exhibited excellent performance because of the synergetic effects that derived from their different components of the hybrid materials.

To solve the problem of Co^{2+}/Co^{3+} redox shuttles and overcome the Pt electrode challenge, and thus promote the Co-mediated DSSCs commercial application, there

are still several key steps needed for the optimization of PCE in the future: 1). the Co^{2+}/Co^{3+} redox shuttles present superior performances of dye regeneration, however, the larger size of the Co^{2+}/Co^{3+} redox shuttles results in the lower ion mobility. Therefore, the novel approach of using tandem-redox electrolyte solution, especially using other redox shuttles, may improve the performance of DSSCs; 2). the inefficient charge transfer of the Co^{2+}/Co^{3+} redox shuttles at the CE also limits the PCE. Therefore, optimizing structure of Pt-free CE catalysts further improve their performance. Meanwhile, the properties of Pt-free CE catalysts should be matched with the Co^{2+}/Co^{3+} redox shuttles; 3). the stability of Co-mediated DSSCs limits the applications in practice. Facile deposition techniques with enhanced stabilities will improve the possibility of commercial applications of Co-mediated DSSCs; 4). detailed mechanistic understanding of Co-mediated DSSCs is vital to developing novel CE catalytic materials and processes that can be used to drive them in affordable and sustainable methods; 5) considering the practical application, solid state DSSCs should be given more attention in future.

Acknowledgements

Projects in the National Science & Technology Pillar Program during the Twelfth Five-year Plan Period (2012BAD47B02), Shaanxi Provincial Department of Education (2013JK0927) and Sci-Tech R&D Program of Shaanxi Province (2011JM6010, 2015JM5183) are highly acknowledged. The Project was partly sponsored by SRF for ROCS, SEM.

Notes and references

1. B. O'Regan and M. Grätzel, *Nature*, 1991, **353**, 737-740.
2. M. Wu and T. Ma, *The Journal of Physical Chemistry C*, 2014, **118**, 16727-16742.
3. Y. Chiba, A. Islam, Y. Watanabe, R. Komiya, N. Koide and L. Han, *Japanese Journal of Applied Physics*, 2006, **45**, L638.
4. H. Nusbaumer, S. M. Zakeeruddin, J.-E. Moser and M. Grätzel, *Chemistry-A European Journal*, 2003, **9**, 3756-3763.
5. Q. Wang, S. Ito, M. Grätzel, F. Fabregat-Santiago, I. Mora-Sero, J. Bisquert, T. Bessho and H. Imai, *The Journal of Physical Chemistry B*, 2006, **110**, 25210-25221.
6. S. Yanagida, Y. Yu and K. Manseki, *Accounts of Chemical Research*, 2009, **42**, 1827-1838.
7. M. Wang, N. Chamberland, L. Breau, J.-E. Moser, R. Humphry-Baker, B. Marsan, S. M. Zakeeruddin and M. Grätzel, *Nature Chemistry*, 2010, **2**, 385-389.
8. G. Boschloo and A. Hagfeldt, *Accounts of Chemical Research*, 2009, **42**, 1819-1826.
9. H. Nusbaumer, S. M. Zakeeruddin, J. E. Moser and M. Grätzel, *Chemistry-A European Journal*, 2003, **9**, 3756-3763.
10. S. A. Sapp, C. M. Elliott, C. Contado, S. Caramori and C. A. Bignozzi, *Journal of the American Chemical Society*, 2002, **124**, 11215-11222.
11. H. Wu, Z. Lv, Z. Chu, D. Wang, S. Hou and D. Zou, *Journal of Materials Chemistry*, 2011, **21**, 14815-14820.
12. L. Wang, E. W.-G. Diau, M. Wu, H.-P. Lu and T. Ma, *Chemical Communications*, 2012, **48**, 2600-2602.
13. G. Oskam, B. V. Bergeron, G. J. Meyer and P. C. Searson, *The Journal of Physical Chemistry B*, 2001, **105**, 6867-6873.
14. P. Wang, S. M. Zakeeruddin, J.-E. Moser, R. Humphry-Baker and M. Grätzel, *Journal of the American Chemical Society*, 2004, **126**, 7164-7165.
15. F. Hao, P. Dong, Q. Luo, J. Li, J. Lou and H. Lin, *Energy & Environmental Science*, 2013, **6**, 2003-2019.
16. J. Wu, Z. Lan, J. Lin, M. Huang, Y. Huang, L. Fan and G. Luo, *Chemical Reviews*, 2015, **115**, 2136-2173.
17. H. Wang, P. G. Nicholson, L. Peter, S. M. Zakeeruddin and M. Grätzel, *The Journal of Physical Chemistry C*, 2010, **114**, 14300-14306.
18. P. J. Cameron, L. M. Peter, S. M. Zakeeruddin and M. Grätzel, *Coordination Chemistry Reviews*, 2004, **248**, 1447-1453.
19. S. M. Feldt, E. A. Gibson, E. Gabrielsson, L. Sun, G. Boschloo and A. Hagfeldt, *Journal of the American Chemical Society*, 2010, **132**, 16714-16724.
20. S. Mathew, A. Yella, P. Gao, R. Humphry-Baker, B. F. Curchod, N. Ashari-Astani, I. Tavernelli, U. Rothlisberger, M. K. Nazeeruddin and M. Grätzel, *Nature Chemistry*, 2014.
21. P. J. Cameron, L. M. Peter, S. M. Zakeeruddin and M. Grätzel, *Coordination Chemistry Reviews*, 2004, **248**, 1447-1453.
22. M. Liberatore, A. Petrocco, F. Caprioli, C. La Mesa, F. Decker and C. A. Bignozzi, *Electrochimica Acta*, 2010, **55**, 4025-4029.
23. J.-H. Yum, E. Baranoff, F. Kessler, T. Moehl, S. Ahmad, T. Bessho, A. Marchioro, E. Ghadiri, J.-E. Moser and C. Yi, *Nature Communications*, 2012, **3**, 631.
24. S. Yun, A. Hagfeldt and T. Ma, *Advanced Materials*, 2014, **26**, 6210-6237.

25. S. Thomas, T. Deepak, G. Anjusree, T. Arun, S. V. Nair and A. S. Nair, *Journal of Materials Chemistry A*, 2014, **2**, 4474-4490.
26. L. Kavan, J.-H. Yum and M. Grätze, *Electrochimica Acta*, 2014, **128**, 349-359.
27. L. Kavan, *Top Curr Chem*, 2014, **348**, 53-94.
28. S. Ahmad, E. Guillén, L. Kavan, M. Grätzel and M. K. Nazeeruddin, *Energy & Environmental Science*, 2013, **6**, 3439-3466.
29. S. Ahmad, T. Bessho, F. Kessler, E. Baranoff, J. Frey, C. Yi, M. Grätzel and M. K. Nazeeruddin, *Physical Chemistry Chemical Physics*, 2012, **14**, 10631-10639.
30. J. D. Roy-Mayhew and I. A. Aksay, *Chemical Reviews*, 2014, **114**, 6323-6348.
31. N. Papageorgiou, W. Maier and M. Grätzel, *Journal of the Electrochemical Society*, 1997, **144**, 876-884.
32. Y.-L. Lee, C.-L. Chen, L.-W. Chong, C.-H. Chen, Y.-F. Liu and C.-F. Chi, *Electrochemistry Communications*, 2010, **12**, 1662-1665.
33. G. Calogero, P. Calandra, A. Irrera, A. Sinopoli, I. Citro and G. Di Marco, *Energy & Environmental Science*, 2011, **4**, 1838-1844.
34. L. Kavan, J.-H. Yum and M. Grätzel, *ACS Applied Materials & Interfaces*, 2012, **4**, 6999-7006.
35. L. Kavan, J.-H. Yum and M. Grätzel, *Nano Letters*, 2011, **11**, 5501-5506.
36. A. Yella, H.-W. Lee, H. N. Tsao, C. Yi, A. K. Chandiran, M. K. Nazeeruddin, E. W.-G. Diau, C.-Y. Yeh, S. M. Zakeeruddin and M. Grätzel, *Science*, 2011, **334**, 629-634.
37. E. Olsen, G. Hagen and S. Eric Lindquist, *Solar Energy Materials and Solar Cells*, 2000, **63**, 267-273.
38. H. Tian, Z. Yu, A. Hagfeldt, L. Kloo and L. Sun, *Journal of the American Chemical Society*, 2011, **133**, 9413-9422.
39. K. Aitola, J. Halme, S. Feldt, P. Lohse, M. Borghei, A. Kaskela, A. G. Nasibulin, E. I. Kauppinen, P. D. Lund, G. Boschloo and A. Hagfeldt, *Electrochimica Acta*, 2013, **111**, 206-209.
40. Y. Li, Q. Feng, H. Wang, G. Zhou and Z.-S. Wang, *Journal of Materials Chemistry A*, 2013, **1**, 6342-6349.
41. H. Zhou, Y. Shi, Q. Dong, L. Wang, H. Zhang and T. Ma, *RSC Advances*, 2014, **4**, 42190-42196.
42. H. Wang, Q. Feng, F. Gong, Y. Li, G. Zhou and Z.-S. Wang, *Journal of Materials Chemistry A*, 2013, **1**, 97-104.
43. S. Caramori, J. Husson, M. Beley, C. A. Bignozzi, R. Argazzi and P. C. Gros, *Chemistry-A European Journal*, 2010, **16**, 2611-2618.
44. J. Cong, Y. Hao, L. Sun and L. Kloo, *Advanced Energy Materials*, 2014, **4**, 1-6.
45. L. Kavan, J.-H. Yum, M. K. Nazeeruddin and M. Grätzel, *ACS Nano*, 2011, **5**, 9171-9178.
46. J. D. Roy-Mayhew, G. Boschloo, A. Hagfeldt and I. A. Aksay, *ACS Applied Materials & Interfaces*, 2012, **4**, 2794-2800.
47. F. Ghamouss, R. Pitson, F. Odobel, M. Boujtita, S. Caramori and C. A. Bignozzi, *Electrochimica Acta*, 2010, **55**, 6517-6522.
48. Y. Li, H. Wang, Q. Feng, G. Zhou and Z.-S. Wang, *ACS Applied Materials & Interfaces*, 2013, **5**, 8217-8224.
49. Z. Wang, H. Xu, Z. Zhang, X. Zhou, S. Pang and G. Cui, *Chinese Journal of Chemistry*, 2014,

491-497.
50. S. K. Swami, N. Chaturvedi, A. Kumar, R. Kapoor, V. Dutta, J. Frey, T. Moehl, M. Grätzel, S. Mathew and M. K. Nazeeruddin, *Journal of Power Sources*, 2015, **275**, 80-89.
51. H. N. Tsao, J. Burschka, C. Yi, F. Kessler, M. K. Nazeeruddin and M. Grätzel, *Energy & Environmental Science*, 2011, **4**, 4921-4924.
52. H. Ellis, N. Vlachopoulos, L. Häggman, C. Perruchot, M. Jouini, G. Boschloo and A. Hagfeldt, *Electrochimica Acta*, 2013, **107**, 45-51.
53. M. Stefik, J.-H. Yum, Y. Hu and M. Grätzel, *Journal of Materials Chemistry A*, 2013, **1**, 4982-4987.
54. M. Al-Mamun, J.-Y. Kim, Y.-E. Sung, J.-J. Lee and S.-R. Kim, *Chemical Physics Letters*, 2013, **561**, 115-119.
55. J. He, J. M. Pringle and Y.-B. Cheng, *The Journal of Physical Chemistry C*, 2014.
56. A. Kay and M. Grätzel, *Solar Energy Materials and Solar Cells*, 1996, **44**, 99-117.
57. L. Kavan, J. H. Yum and M. Grätzel, *ACS Nano*, 2010, **5**, 165-172.
58. H. C. Schniepp, J.-L. Li, M. J. McAllister, H. Sai, M. Herrera-Alonso, D. H. Adamson, R. K. Prud'homme, R. Car, D. A. Saville and I. A. Aksay, *The Journal of Physical Chemistry B*, 2006, **110**, 8535-8539.
59. K. N. Kudin, B. Ozbas, H. C. Schniepp, R. K. Prud'Homme, I. A. Aksay and R. Car, *Nano Letters*, 2008, **8**, 36-41.
60. H. C. Schniepp, K. N. Kudin, J.-L. Li, R. K. Prud'homme, R. Car, D. A. Saville and I. A. Aksay, *ACS Nano*, 2008, **2**, 2577-2584.
61. J. D. Roy-Mayhew, D. J. Bozym, C. Punckt and I. A. Aksay, *ACS Nano*, 2010, **4**, 6203-6211.
62. R. Levy and M. Boudart, *Science*, 1973, **181**, 547-549.
63. S. Oyama, *Catalysis Today*, 1992, **15**, 179-200.
64. M. Wu, X. Lin, A. Hagfeldt and T. Ma, *Chemical Communications*, 2011, **47**, 4535-4537.
65. X. Lin, M. Wu, Y. Wang, A. Hagfeldt and T. Ma, *Chemical Communications*, 2011, **47**, 11489-11491.
66. S. Yun, H. Zhou, L. Wang, H. Zhang and T. Ma, *Journal of Materials Chemistry A*, 2013, **1**, 1341-1348.
67. S. Yun, M. Wu, Y. Wang, J. Shi, X. Lin, A. Hagfeldt and T. Ma, *ChemSusChem*, 2013, **6**, 411-416.
68. S. Yun, L. Wang, C. Zhao, Y. Wang and T. Ma, *Physical Chemistry Chemical Physics*, 2013, **15**, 4286-4290.
69. S. Yun, L. Wang, W. Guo and T. Ma, *Electrochemistry Communications*, 2012, **24**, 69-73.
70. S. Yun, H. Pu, J. Chen, A. Hagfeldt and T. Ma, *ChemSusChem*, 2014, **7**, 442-450.
71. S. Yun, H. Zhang, H. Pu, J. Chen, A. Hagfeldt and T. Ma, *Advanced Energy Materials*, 2013, **3**, 1407-1412.
72. S. Yun, A. Hagfeldt and T. Ma, *ChemCatChem*, 2014, **6**, 1584-1588.

Table of content

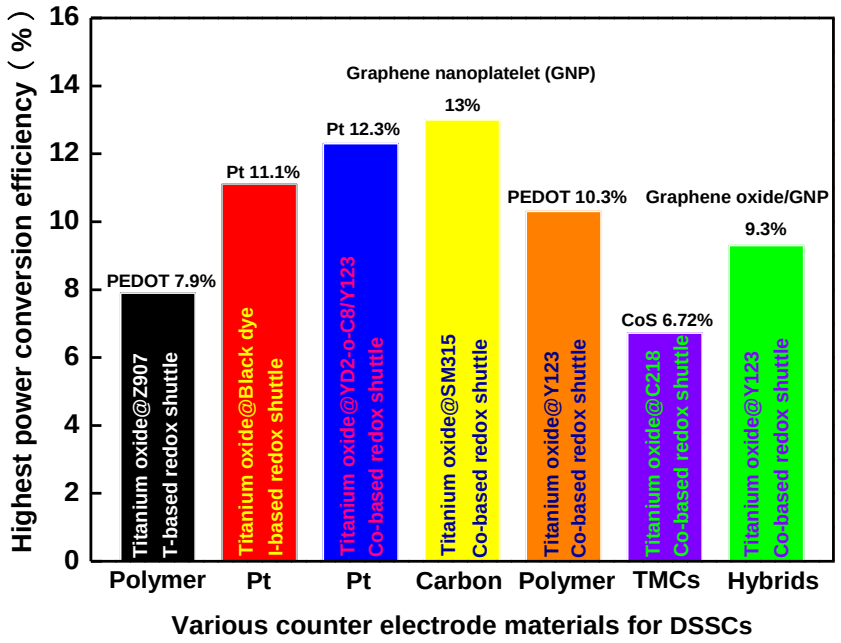

The novel Co-mediated DSSCs with unparalleled merits have so far achieved the highest PCE value for liquid electrolyte DSSCs.